SHOCK, Vol. 58, No. 1, pp. 78–89, 2022

OPEN

ACTIVATION OF THE MITOCHONDRIAL ANTIVIRAL SIGNALING PROTEIN (MAVS) FOLLOWING LIVER ISCHEMIA/REPERFUSION AND ITS EFFECT ON INFLAMMATION AND INJURY

Menachem Ailenberg, Andras Kapus, Chung Ho Leung, Katalin Szaszi, Philip Williams, Caterina diCiano-Oliveira, John C. Marshall, and Ori D. Rotstein

Keenan Research Centre for Biomedical Science of St. Michael's Hospital and the Departments of Surgery, St. Michael's Hospital and the University of Toronto

Received 22 Feb 2022; first review completed 14 Mar, 2022; accepted in final form 9 May 2022

ABSTRACT—Resuscitation of trauma patients after hemorrhagic shock causes global I/R, which may contribute to organ dysfunction. Oxidative stress resulting from I/R is known to induce signaling pathways leading to the production of inflammatory molecules culminating in organ dysfunction/injury. Our recent work demonstrated that oxidative stress was able to induce activation of the mitochondrial antiviral signaling protein (MAVS), a protein known to be involved in antiviral immunity, in an *in vitro* model. We therefore hypothesized that the MAVS pathway might be involved in I/R-induced inflammation and injury. The present studies show that MAVS is activated *in vivo* by liver I/R and *in vitro* in RAW 264.7 cells by hypoxia/reoxygenation (H/R). We utilized both *in vivo* (liver I/R in MAVS knockout mice) and *in vitro* (MAVS siRNA in RAW 264.7 cells followed by H/R) models to study the role of MAVS activation on downstream events. *In vivo*, we demonstrated augmented injury and inflammation in MAVS knockout mice compared with wild-type animals; as shown by increased hepatocellular injury, induction of hepatocyte apoptosis augmented plasma TNF-α levels. Further, *in vitro* silencing of MAVS by specific siRNA in RAW 264.7 and exposure of the cells to H/R caused activation of mitophagy. This may represent a compensatory response to increased liver inflammation. We conclude that activation of MAVS by hypoxia/reoxygenation dampens inflammation, potentially suggesting a novel target for intervention.

KEYWORDS—Autophagy; hypoxia/reoxygenation; liver I/R; MAVS; mitophagy

ABBREVIATIONS—MAVS—mitochondrial antiviral signaling protein; H/R—hypoxia/reoxygenation; RLRs—retinoic acid–inducible gene I (RIG-I)–like receptors

INTRODUCTION

Innate immunity plays a central role in the recognition and elimination of invading pathogens. Recognition of microbes may involve the detection of conserved microbial molecular patterns by a number of pattern recognition receptors, including those that are on the cell surface such as Toll-like receptors and others that are cytosolic, for example, retinoic acid–inducible gene I (RIG-I)–like receptors (RLRs). The RLR signaling pathways are initiated by the recognition of double-stranded viral RNA by one of two cytosolic sensors, namely, RIG-I and MDA5. This interaction induces a conformational change leading to homotypic interaction between the caspase activation and recruitment domain (CARD) of RIG-I and that of the mitochondrial antiviral signaling protein (MAVS), a mitochondrial outer membrane–anchored adaptor protein. The ensuing aggregation and oligomerization of MAVS play a critical role in the antiviral response of eukaryotic cells, as it serves as a platform for downstream activation of type 1 interferons and nuclear factor κB. Together, these promote a cellular antiviral response and viral clearance (1). Recent studies have demonstrated other downstream events related to viral-induced MAVS activation including apoptosis *via* interaction with caspase-8 to mediate caspase-3 activation (2), activation of the NLRP3 inflammasome pathway *via* its role in localization of NLRP3 to the mitochondria (3), and mitochondrial autophagy by its interaction with the autophagy receptor LC3 (4). Together, these connections suggest a broader role for MAVS in regulation of cellular homeostasis.

Oxidative stress seems to play a role in the activation of MAVS. Consistent with the proposed canonical pathway involving virus interactions with RLRs, mitochondrial reactive oxygen species (ROS) generated by the respiratory chain inhibitor rotenone increased expression of MAVS *via* activation of RLR (5). In addition, we and others have demonstrated a role for ROS in MAVS activation that was independent of RIG-I (6,7). This suggests the possibility that other pathological processes involving generation of ROS might involve MAVS activation in modulating downstream events. One such process is I/R injury wherein generation of ROS is important in mediating cellular/tissue inflammation and injury. For example, liver injury following I/R is known to involve the generation of ROS, both by cells residing in the liver and by infiltrating cells such as neutrophils (8). Based on the observation that oxidative stress is able to induce MAVS activation and initiation of downstream inflammatory pathways, we hypothesized a potential role for MAVS activation in liver I/R injury. In the present article, we show that MAVS is activated *in vitro* by exposing cells to a hypoxia/reoxygenation (H/R) stimulus and also *in vivo* using a murine model of liver I/R. Interestingly, MAVS activation seems to dampen liver injury induced by I/R.

Address reprint requests to Ori D. Rotstein, MD, MSc, St. Michael's Hospital, 30 Bond St, LKSKI 3-305, Toronto, Ontario, Canada M5B 1W8. E-mail: ori.rotstein@unityhealth.to

This work was supported by the Canadian Institutes for Health Research to O.D.R. (23766), the Keenan Chair in Research Leadership, and The Natural Sciences and Engineering Research Council of Canada to A.K. (RGPIN227-908-13).

The authors report no conflicts of interest.

Supplemental digital content is available for this article. Direct URL citation appears in the printed text and is provided in the HTML and PDF versions of this article on the journal's Web site (www.shockjournal.com).

DOI: 10.1097/SHK.0000000000001949

MATERIALS AND METHODS

Reagents and antibodies

All reagents were purchased from Sigma-Aldrich (Oakville, Ontario, Canada) unless otherwise stated. Primary antibodies were purchased from Cell Signaling (Pickering, Ontario, Canada), Santa Cruz Biotechnology (SCBT, Paso Robles, CA), or NanoTools (Teningen, Germany). Horseradish peroxidase–conjugated anti–rabbit or anti–mouse secondary antibodies were from Jackson Immuno Research Laboratories (West Grove, PA). Anti–rabbit Alexa Fluor 488 immunoglobulin G was a product of Molecular Probes (Life Technologies Inc., Burlington, Ontario, Canada). MAVS rodent-specific antibody and blocking peptide were from Cell Signaling (see Supplemental Digital Content 1, http://links.lww.com/SHK/B451, for antibody evaluation). Hoechst nuclear dye was from Cell Signaling. Transfection reagent jetPRIME was from Polyplus Transfection (New York, NY). NucView 488 Caspase-3 enzyme substrate was purchased from Biotum (Fremont, CA). The substrate consists of a fluorogenic DNA dye and a DEVD substrate moiety specific for caspase-3/7. The substrate, which is both nonfluorescent and nonfunctional as a DNA dye, rapidly crosses cell membranes to enter the cytoplasm, where it is cleaved by caspase-3 to form a high-affinity DNA dye that stains the nucleus bright green. Plasmid pBabe. hygro-mCherry-GFP FIS (101–152) was purchased from MRC PPU Reagents and Services (Dundee, Scotland). Hygromycin B was purchased from Bioshop Canada Inc (Burlington, Ontario, Canada). MitoTracker Red CMXRos was purchased from Molecular Probes (Eugene, OR).

Cell culture and transfection

The murine macrophage RAW 264.7 cell line was purchased from ATCC (Manassas, VA) or Sigma and maintained in Dulbecco modified eagle medium (DMEM) containing 10% fetal bovine serum (FBS) as previously described (6). Cells were passaged every week for a maximum of 15 passages. For all experiments, 24 hours after plating, cells were starved in 2% FBS for 24 hours before starting the experiment. As needed, plasmids, polyinosinic acid:polycytidylic acid (poly I:C) or siRNA was transfected using jetPRIME reagent according to the manufacturer's recommendations. Plasmid Mito-RFP (Clontech, Mountain View, CA) was used at 1 μg/mL overnight. Poly I:C was then transfected at 5 μg/mL overnight. The next day, cells were fixed and subjected to immunofluorescence (see below).

For imaging, cells were fixed and subjected to immunocytochemistry. Images were taken using Zeiss LSM 700 inverted confocal microscope (Carl Zeiss Canada Ltd., Toronto, ON, Canada), Quorum Spinning Disc with TIRF (Quorum Technologies Inc., Puslinch, Ontario, Canada), or Olympus IX81 fluorescent microscope (Olympus Canada Inc, Richmond Hill, ON, Canada). For imaging, cells were fixed and subjected to immunocytochemistry. Images were taken using Zeiss LSM 700 inverted confocal microscope, Quorum Spinning Disc with TIRF (Quorum Technologies Inc.) or Olympus IX81 fluorescent microscope. For the Spinning Disc, we used a z-step size of 0.2 to 0.3 μm. Surface renderings of MAVS and Mito-RFP were performed using Imaris v8.2 (Oxford Instruments Group, Abingdon, Oxfordshire, England). All settings for surface rendering were kept constant in order to allow for comparison between experimental conditions. Under normal conditions, MAVS is evenly distributed on the mitochondria surface (IF, green). After activation, MAVS migrates and exposes the mitochondria surface as indicated by red Mito-RFP.

Nuclear staining was performed using Hoechst 33342 (Life Technologies Inc.). Mitochondrial staining with MitoTracker Red was performed on live cells (100 μM for 30 minutes at 37°C), fixed, and processed as mentioned previously.

Mitophagy assay

We evaluated mitophagy in a stable RAW 264.7 cell line expressing plasmid pBabe.hygro-mCherry-GFP FIS 101–152, as reported by Allen et al. (9). The assay consists of cells expressing a tandem mCherry–GFP tag attached to the outer mitochondrial membrane localization signal of the protein FIS1 (residues 101–152). When expressed on intact mitochondria, both red and green signals are detected. Under the acidic condition of the lysosome, the green signal is quenched. Thus, signals in the red channel that are not colocalized with signals in the green channel represent mitophagolysosome. To construct the RAW 264.7 stable cell line, we first transfected GP2-293 cells (HEK in cis gag-pol) with the transfer vector (pBabe.hygro-mCherry-GFP FIS 101–152) and the envelope plasmid p10A1 using jetPRIME reagent. The harvested virus was used to transduce RAW 264.7 cells. Cells were selected with 500 μg/mL hygromycin B and cloned by minimal dilution. As a positive control, we tested the impact of the mitochondrial uncoupler CCCP, a known autophagy inducer, on the two fluorescence signals. As expected, we observed the formation of red puncta (without green fluorescence) in the treated cells compared with the dimethyl sulfoxide (DMSO)–treated control (Figure, Supplemental Digital Content 2, http://links.lww.com/SHK/B452). To quantify mitophagy, red puncta in cells expressing more than three puncta, with no green signal in the green channel, were counted in three representative fields for each treatment. This number was divided by the total cell numbers in the field and expressed as total mitophagolysosome per cell. This value was than normalized to the control value, and mean ± SEM was calculated for three separate experiments. Mitophagy images were evaluated by two independent researchers.

Measuring caspase-3 expression using NucView 488

RAW cells were plated in 96-well plates in 10% FBS in DMEM. For each treatment, cells were plated in triplicate wells. On the next day, cells were transfected with control or MAVS siRNA (final concentration 10 nM; Qiagen, Valencia, CA) in 2% FBS in DMEM using jetPRIME reagent. On the next day, media were changed to 10% FBS in DMEM for 6 hours. Media were then changed to 5% FBS in phenol red–free DMEM containing 2.5 μM (final concentration) NucView 488 Caspase 3 Enzyme substrate (Biotum) and incubated under normal or hypoxia conditions. After 18 hours, cells were transferred to normoxia and treated with Hoechst (1 μg/mL final concentration) for 4 hours. For positive control, cells were also treated with staurosporine (STSP) (1 μM final concentration) for 4 hours. In some experiments, cells were fixed and subjected to immunofluorescence using MAVS first antibody and anti–rabbit Alexa 568 second antibody (red). Therefore, caspase-3–expressing cells have green-stained nuclei and when merged with nuclei of Hoechst blue–stained cells reveal turquoise-stained nuclei. Nine regions in each well were read for blue (Hoechst), green (NucView 488 Caspase-3), red (MAVS), and phase contrast, using ImageXpress Micro apparatus (Molecular Devices, San Jose, CA). Thus, a few thousand cells were analyzed for each well in triplicate treatment. Caspase-3 activity was expressed as percentage of NucView 488–positive cell and nuclear Hoechst-stained cells. MAVS expression was measured as mean cell average Alexa 568 fluorescent intensity. The utility of NucView 488 was also assessed with confocal microscopy. For confocal microscopy, cells were plated on coverslips. On the next day, cells were treated overnight with NucView 488 Caspase-3 and then were treated directly with Hoechst, STSP, or DMSO for 2 hours. Cells were subjected to immunocytochemistry for MAVS and three-dimensional (3D) rendering as described previously.

We validated the utility of the NucView 488 reagent under normoxia condition by treating the cells for 2 hours with STSP (Figure, Supplemental Digital Content 3, http://links.lww.com/SHK/B453). Staurosporine caused a strong activation of caspase-3 as manifested by a green nuclear staining. It is interesting to note that apoptotic (turquoise nuclei) cells are low (green arrow) or devoid of MAVS (red signal), whereas nonapoptotic cells (blue nuclei) express high levels of MAVS (red signal; red arrow).

We evaluated the STSP effect using three methods for quantitation: (1) ImageXpress, (2) fluorescent plate reader, and (3) Fiji (ImageJ, National Institutes of Health, Bethesda, Maryland, USA) nuclear area measurement. The most robust and representative quantitation method was ImageXpress, and therefore, we proceeded to use this method in our experiments.

Hypoxia-reoxygenation experiments

RAW cells were subjected to hypoxia (85% N_2:10% H_2:5% CO_2) for 18 hours in a Forma Anaerobic System apparatus (Thermo Fisher Scientific, Mississauga, Ontario, Canada) and then reoxygenated under normoxic conditions (95% air:5% CO_2) for up to 4 hours. Control cells were incubated for 22 hours under normoxic conditions.

Liver I/R in control and MAVS knockout mice

All mice were maintained under pathogen-free conditions in St. Michael's Hospital's (SMH) vivarium. We used male mice because the degree of hepatic injury in male mice is consistently more severe than female mice following I/R, and thus, using males alone was intended to lessen the variability. Animal experiments were approved by SMH's animal research committee and performed in accordance with SMH's guidelines for animal care and use. Wild-type control mice (B6129SF2/J) were purchased from The Jackson Laboratory (Bar Harbor, Maine) (stock no. 101045). MAVS knockout (KO) breeding pairs (The Jackson Laboratory, stock no. 008634) were bred at the SMH vivarium and kept under sterile conditions. At least four mice were used in each treatment group except in a complex experiment where multiple time points and two mice types (WT and KO) were studied. In this case, three to six mice were used for the various time points or mice types.

We validated the MAVS antibody, MAVS siRNA, and MAVS KO mice using Western immunoblots, semidenaturing detergent-agarose gel electrophoresis (SDD-AGE), confocal microscopy, and reverse transcriptase–polymerase chain reaction (RT-PCR) (see legend to Figure, Supplemental Digital Content 1, http://links.lww.com/SHK/B451, for elaborate protocols).

Liver I/R was performed in MAVS KO and wild-type mice as previously described (10). Male mice, 7 to 9 weeks old, were anesthetized with isoflurane, and warm partial liver ischemia was accomplished by placing an atraumatic clamp on the hepatic portal vein and arterial branches to the left and median lobes for 45 minutes. Reperfusion was initiated with removal of the clamp, and animals were killed at 1, 2, and 4 hours after reperfusion. Sham-operated animals underwent laparotomy and vessel exposure but without clamp application. MitoTEMPO (10 mg/kg) and apocynin (10 mg/kg) were dissolved in DMSO and phosphate-buffered saline

(PBS), respectively, and injected intraperitoneally 15 minutes before liver ischemia. Vehicle control animals were injected with DMSO or PBS alone. Blood and liver tissue were harvested for evaluation of hepatic injury and inflammation. Plasma alanine transaminase (ALT) levels as a marker of hepatocellular injury were measured in blood samples taken at varying time points after reperfusion by the Diagnostic Laboratory at SMH. Plasma levels of TNF-α were quantitated in blood samples using commercially available enzyme-linked immunosorbent assay kits according to the manufacturer's instructions (R&D Systems, Minneapolis, MN).

Sodium dodecyl sulfate–polyacrylamide gel electrophoresis and Western blotting

Cells were lysed with lysis buffer and subjected to Western blotting. Protein concentrations were measured using DC protein assay (Bio-Rad Laboratories, Mississauga, Ontario, Canada), and equal protein amounts were loaded on gel. Gel loading was assessed with probing for glyceraldehyde 3-phosphate dehydrogenase (GAPDH) or corresponding nonphosphorylated proteins. Blots where proteins were migrating at a distance from each other were cut across guided by prestained protein ladder (FroggaBio Inc., Toronto, Ontario, Canada) and probed with the specific antibody. When proteins of interest were close to each other, blots were stripped and reprobed with the specific antibody. Protein signals were developed using ECL, ECL Prime (GE Healthcare Life Sciences, Baie d'Urfe, Quebec, Canada) or UltraScence (FroggaBio Inc.) and captured on film or ChemiDoc Touch Imaging System (Bio-Rad Laboratories). Protein signal intensities on film were compared by using GS Calibrated Densitometer (Bio-Rad Laboratories), and ChemiDoc Touch signals were analyzed with Image Lab (Bio-Rad Laboratories).

Semidenaturing detergent-agarose gel electrophoresis

To preserve and measure high-molecular-weight aggregates, SDD-AGE was used with modifications (6). Briefly, cell extracts were incubated at room temperature for 5 minutes with 0.5% sodium dodecyl sulfate (SDS) (final concentration) followed by addition of 6× DNA loading dye (Fermentas, Burlington, Ontario, Canada). Samples were loaded on 1.5% agarose gel containing 0.1% SDS and resolved using 1× TBE running buffer containing 0.1% SDS at 100 V in the cold. Protein aggregates were transferred to nitrocellulose paper with PBS using capillary transfer. After transfer, nitrocellulose membrane was subjected to immunoblotting as described previously in the SDS–polyacrylamide gel electrophoresis (PAGE) section.

Polymerase chain reaction for genotyping and mRNA quantification

MAVS KO genotyping was performed on ear notches of mice using REDExtract-N-Amp PCR kit according to the manufacturer recommendation (Sigma-Aldrich). Genomic DNA extracts were subjected to multiplex PCR (primers 5′-AGC CAA GAT TCT AGA AGC TGA GAA-3′; 5′-TAG CTG TGA GGC AGG ACA GGT AAG G-3′; 5′-GTG GAA TGT GTG CGA GGC CAG AGG C-3′). MAVS mRNA levels in wild-type and MAVS KO mice were evaluated using end-point RT-PCR with primers 5′-CGCCGGCCTGGCTGGGTGGA-3′ and 5′-AGGGAGCGGAGTGAGGTCCCCG-3′ (see Figure, Supplemental Digital Content 1E–G, http://links.lww.com/SHK/B451, for evaluation).

For mRNA quantitation using RT–quantitative PCR, total liver RNA was extracted using RNeasy Mini Kit (Qiagen). Livers from at least three mice were used per treatment, and each liver was assayed in triplicates. One microgram RNA was subjected to DNase I treatment to remove genomic DNA and then reverse transcribed (Bio-Rad, Hercules, CA). The relative abundance of mRNA for TNF-α, heme oxygenase-1 (HO-1), IL-10, and GAPDH (endogenous reference control) in the liver was quantified using SYBR green–based quantitative PCR (Applied Biosystems, Foster City, CA). Each reaction was performed on total RNA extracts from three to four animals in each treatment group in triplicates. Real-time PCR conditions were as follows: initial denaturation at 95°C for 10 minutes, followed by 40 cycles of 95°C for 15 seconds, and 60°C for 60 seconds. Primer efficacy was predicted using Umelt (11) and was verified by the melt-curve analysis at the completion of the PCR. Relative abundance of gene expression was calculated by relative quantification $2^{-\Delta\Delta T}$ method, using GAPDH as the endogenous reference control and one of the sham-operated samples as calibrator for the relative quantification. All primers were purchased from Sigma-Aldrich. The sequences of forward and reverse, respectively, primers were as follows:

TNF-α: 5′-TATGGCTCAGGGTCCAACTC-3′ and 5′-CTCCCTTTGCAGA ACTCAGG-3′;

IL-10: 5′-GGCGCTGTCATCGATTTCTC-3′ and 5′-GCCTTGTAGACACC TTGGTCTTG-3′; HO-1: 5′-TAGCCCACTCCCTGTGTTTCCTTT-3′ and

5′-TGCTGGTTTCAAAGTTCAGGCCAC -3′; and

GAPDH: 5′-AGAAACCTGCCAAGTATGATGACA-3′ and 5′TGAAGTCG CAGGAGACAACCT-3′.

Statistical analysis

Data were subjected to one-way ANOVA. Differences between means were evaluated using Tukey-Kramer minimum significant differences, and significance was set to $P = 0.05$. When applicable, means were compared using Student t test. Bars represent mean ± SEM. Asterisks/crosses denote statistical difference compared with control. When individual figures are shown, they are representative of at least three independent studies.

RESULTS

Activation of MAVS by liver I/R and cellular H/R

Evidence of MAVS activation is demonstrated by the formation of high-molecular-weight aggregates in semidenaturing conditions and also by the loss of MAVS protein monomer (6,12). To assess whether MAVS activity is altered by I/R, we subjected mice to liver ischemia for 45 minutes followed by reperfusion for 1 hour. Figure 1A shows the formation of MAVS aggregates following liver I/R (left panel) and the reduction of the MAVS monomer (right panel) as early as 1 hour following reperfusion. Also shown in this blot is the absence of MAVS expression in liver extracts of KO mice, subjected to the same I/R protocol (see below). To mimic I/R *in vitro*, we performed H/R of RAW 264.7 cells. As shown in Figure 1B, H/R similarly induces reduction of MAVS monomers. In addition to examining trypan blue exclusion, protein expression of HO-1, known to be induced in this model, served as a positive control for cellular viability. We also observed morphological changes in MAVS distribution following H/R (Fig. 1C). Cells were transfected with Mito-RFP (red) and subjected to H/R, fixed, and subjected to immunofluorescence using anti-MAVS antibody. In normoxic cells, the mitochondrial network had a typical threadlike appearance, a finding that was mirrored by MAVS immunostaining. In response to H/R, both assumed a more globular appearance. The arrow in the lower panels indicates a cell that was not transfected with Mito-RFP. The bottom right panel shows the merged picture of cells after H/R. The globular morphology of the MAVS protein is observed in the cell not transfected with Mito-RFP (shown with the arrow, upper left of two cells shown) and also in the Mito-RFP transfected cell where the overlay of the MAVS and mitochondria is shown (lower right cell). We then subjected confocal stacked micrographs to 3D rendering to further study the morphology by allowing visualization of the surface structures (Figure, Supplemental Digital Content 4, http://links.lww.com/SHK/B454). Again, the cell not transfected with Mito-RFP is designated with the arrow. In control cells, MAVS appears to be distributed in a manner that covers the Mito-RFP, consistent with its even surface distribution as an outer membrane mitochondrial protein (upper far right panel). Following H/R, the ensuing clustering of MAVS allowed the visualization of the mitochondrial surface (compare upper right to lower right panels). The findings are consistent with the reported aggregation of MAVS protein between adjacent mitochondria following activation with virus (13). In addition, this change in morphology is similar to our previous report where the drug dynasore was used to activate MAVS (6). As further evidence that these changes represented MAVS activation, we studied the effect of synthetic double-stranded RNA, poly I:C, on MAVS activation in RAW cells, as a surrogate for viral infection. The delivery mode of poly I:C can induce distinct downstream pathways. Specifically, addition of poly I:C directly to cells causes endosome-mediated internalization

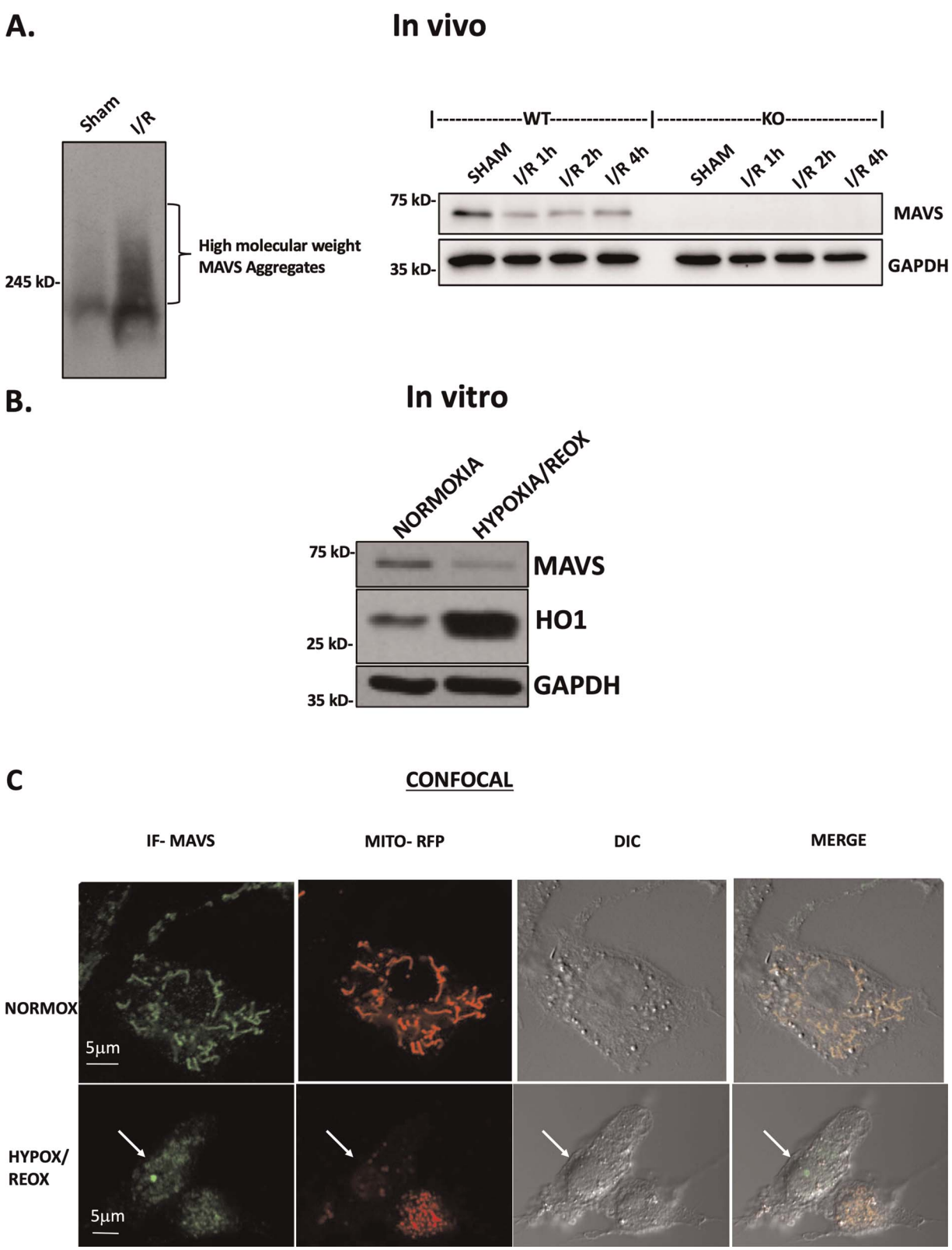

FIG. 1. **MAVS is activated *in vivo* after liver I/R and *in vitro* after H/R in RAW cells.** A, *In vivo*: Left panel, SDD-AGE showing enhanced MAVS aggregates in I/R (45′/1 hour) livers compared with sham-operated mice. Right panel, Western immunoblot showing reduction in MAVS monomer in I/R livers (45′/1–4 hours' reperfusion) compared with sham-operated mice. Blots were also assayed for GAPDH for loading controls. **B**, *In vitro*: Western blot—RAW cells were subjected to 18 hours' hypoxia followed by 4 hours' incubation under normal oxygen levels. Control cells were incubated for the duration of the experiment under normal oxygen levels. Proteins were resolved using SDS-PAGE. Blots were cut across according to the expected molecular sizes and visualized using specific antibodies. Note reduction of MAVS monomer, enhanced HO-1, and no change in GAPDH after hypoxia/reoxygenation. C, Confocal microscopy—RAW cells were plated on glass coverslips, transfected with Mito-RFP plasmid (red) for 24 hours and subjected to hypoxia/reoxygenation regimen as described in section B. Cells were fixed and underwent immunocytochemistry procedure with anti-MAVS primary antibody, and Alexa Fluor 488–labeled secondary antibody (green). Note threadlike typical structure of mitochondria both in Mito-RFP–transfected and MAVS-stained control RAW cells. Note also that following hypoxia/reoxygenation mitochondria, assume more globular shortened structure. Arrow shows untransfected cell. Bars indicate 5 µm.

and activation of TLR3, whereas transfection of cells with poly I:C causes it to interact with cytoplasmic RIG-I and activate the MAVS pathway. Figure 2A demonstrates that transfected poly I:C causes a reduction in MAVS monomer, consistent with its activation, whereas nontransfected poly I:C does not affect MAVS levels. As expected, both strategies caused an increase in phosphorylation of p65 (p-p65) and IRF3 (p-IRF3). Similar to Figure 1C, nontreated control RAW cells exhibited threadlike structure of mitochondria and a similar distribution of MAVS (Fig. 2B). Following transfection with poly I:C, mitochondria and MAVS assumed a globular morphology (Fig. 2B). With 3D rendering of confocal images, the mitochondria from control cells demonstrated near-complete masking of Mito-RFP by even distribution of immunostained MAVS (Figure, Supplemental Digital Content 5, http://links.lww.com/SHK/B455, control merged). However, in poly I:C–transfected cells, mitochondria were revealed through the aggregation of MAVS protein (Figure, Supplemental Digital Content 5, http://links.lww.com/SHK/B455, poly I:C merged). Considered together, these findings provide evidence that MAVS is activated both *in vivo* by liver I/R and *in vitro* by H/R stress.

Oxidative stress contributes to MAVS activation

We have previously shown that induction of ROS in cultured RAW cells caused activation of MAVS in response to dynasore, a reagent often used as an inhibitor of endocytosis (6). Oxidative stress is known to be generated during liver I/R (8). To investigate whether oxidative stress might play a role in MAVS activation following I/R, we treated animals with inhibitors of mitochondrial ROS and inhibitors of the NADPH oxidase before the initiation of liver I/R. As shown in Figure 3A, MAVS activation following I/R, as demonstrated by reduction in the MAVS monomer, was reversed when mice were injected intraperitoneally with mitoTEMPO before liver I/R, but not with the vehicle DMSO. In addition, the inhibitor of NADPH oxidase, apocynin, similarly prevented the activation of MAVS by liver I/R (Fig. 3A). Together, these demonstrate a role of oxidants in MAVS activation by I/R. To gain further insight into the underlying mechanism, we used the *in vitro* H/R system and tested the involvement of Rac1 activation, a pathway known to be connected to downstream activation of NADPH oxidase and mitochondrial oxidants (14,15). Hypoxia/reoxygenation caused an increase in activated Rac1 in RAW cells

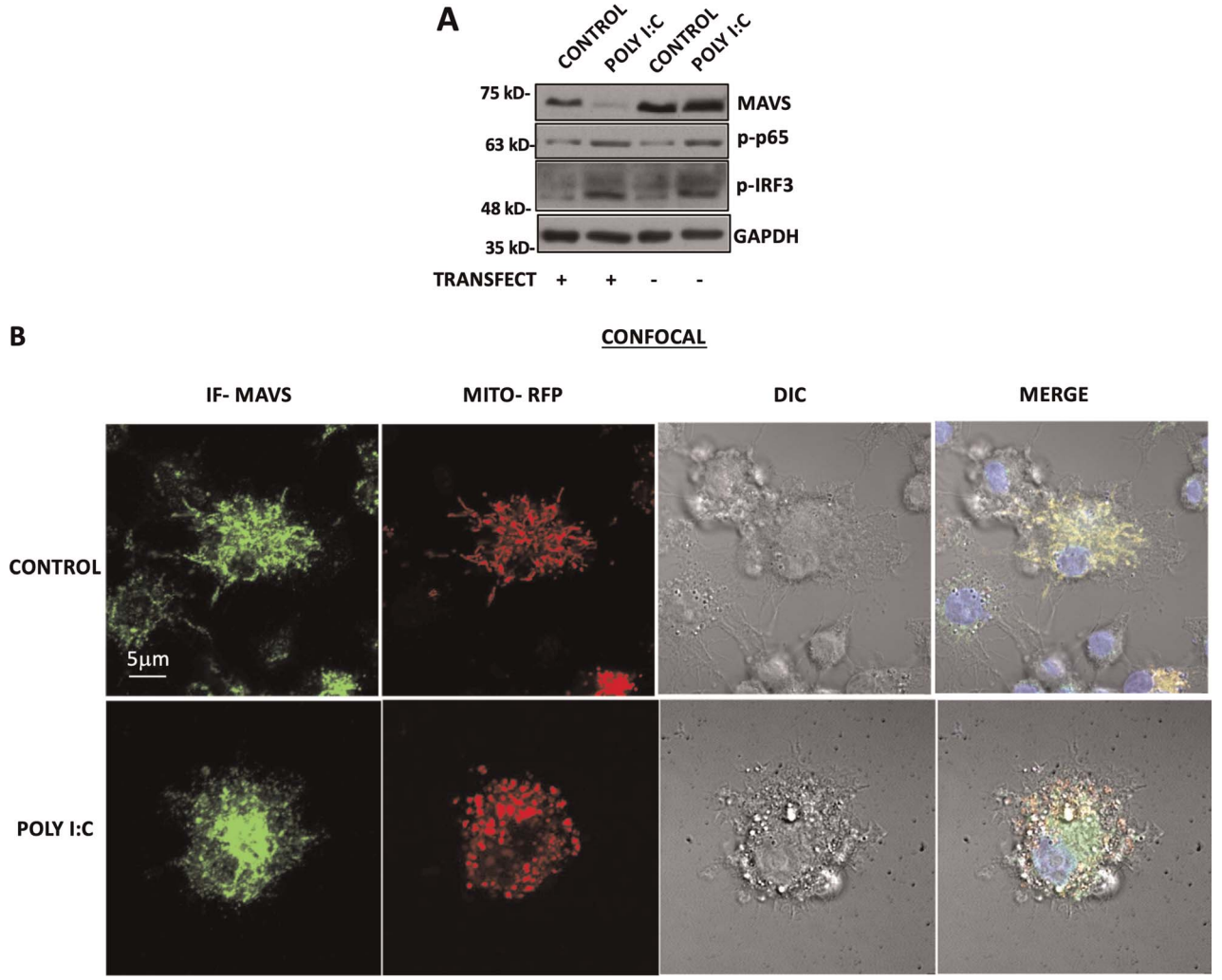

Fig. 2. **Poly I:C activates MAVS in RAW 264.7 cells.** A, Western immunoblot: poly I:C (5 µg/mL) was transfected or added to RAW cells for 18 hours. Cell lysate were subjected to SDS-PAGE and blotted with the indicated antibodies. Note reduction of the MAVS monomer in the poly I:C–transfected but not the added cells, indicating activation of the MAVS pathway. Note also activation of nuclear factor κB (Ser536) and IRF3 (Ser396) with both transfection and addition. B, Immunofluorescence: RAW cells were transfected with Mito-RFP plasmid for 24 hours. On the next day, cells were transfected with poly I:C (5 µg/mL) for 24 hours (control cells were mock-transfected) and stained for MAVS. Note disruption of threadlike mitochondria to short mitochondria after transfection with poly I:C. Note also more mitochondria devoid of MAVS. Bar indicates 5 µm.

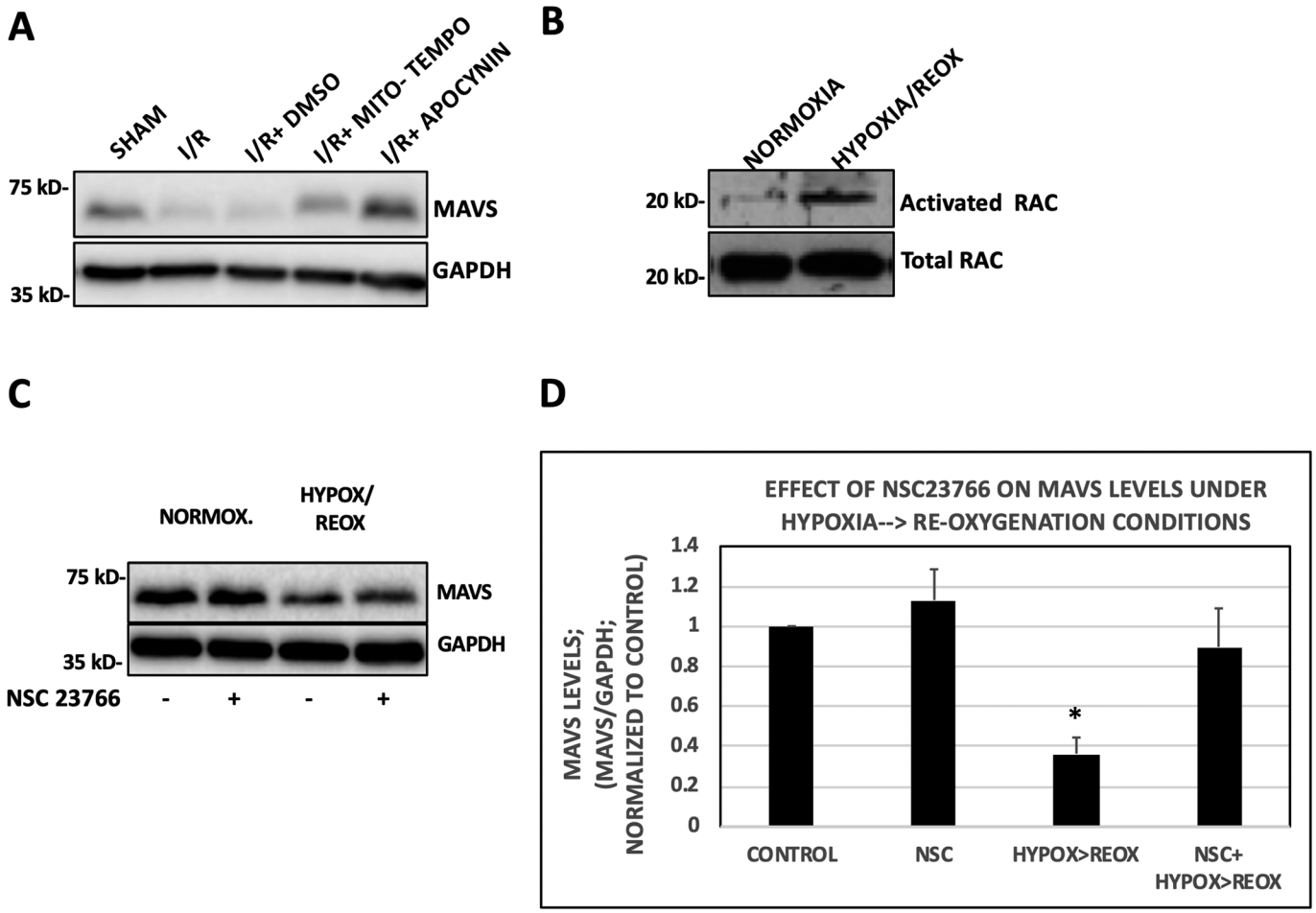

FIG. 3. **Oxidative stress contributes to MAVS activation *in vivo* and *in vitro*.** A, *In vivo*: mice subjected to I/R (45′/1 hour) showed reduced levels of the MAVS monomer in the liver extracts. However, intraperitoneal preinjection of MitoTEMPO (10 mg/kg) or apocynin (10 mg/kg) prevented the reduction of the MAVS monomer following I/R. Blots were probed for GAPDH as loading controls. B, *In vitro*: RAW cells were subjected to hypoxia for 18 hours and then transferred to normoxia condition. Control cells were kept under normoxia conditions for the same duration. RAW cell extracts were subjected to RAC activating assay. Blots were processed also for total RAC as loading controls. C, RAW cells were treated with or without 10 μM NSC23766 Rac1–specific inhibitor and incubated for 18 hours with or without hypoxia conditions. Cells were then incubated for additional 4 hours under normal conditions and subjected to Western immunoblotting for MAVS or GAPDH. D, Densitometry depicting results of seven separate studies is shown. MAVS activation is inhibited by the Rac1 inhibitor. ANOVA, n = 7, **Post hoc P* < 0.05 vs. other groups.

(Fig. 3B). The specific Rac inhibitor, NSC23766 (10 μM), prevented the reduction in MAVS monomer, consistent with a role of activated Rac1 in MAVS activation (representative blot in Fig. 3C and quantitation of seven independent studies in Fig. 3D).

Liver I/R injury is increased in MAVS KO animals

Having demonstrated MAVS activation by liver I/R, we explored the role of MAVS in liver injury using MAVS KO mice. To evaluate the role of MAVS in I/R-induced liver injury, we

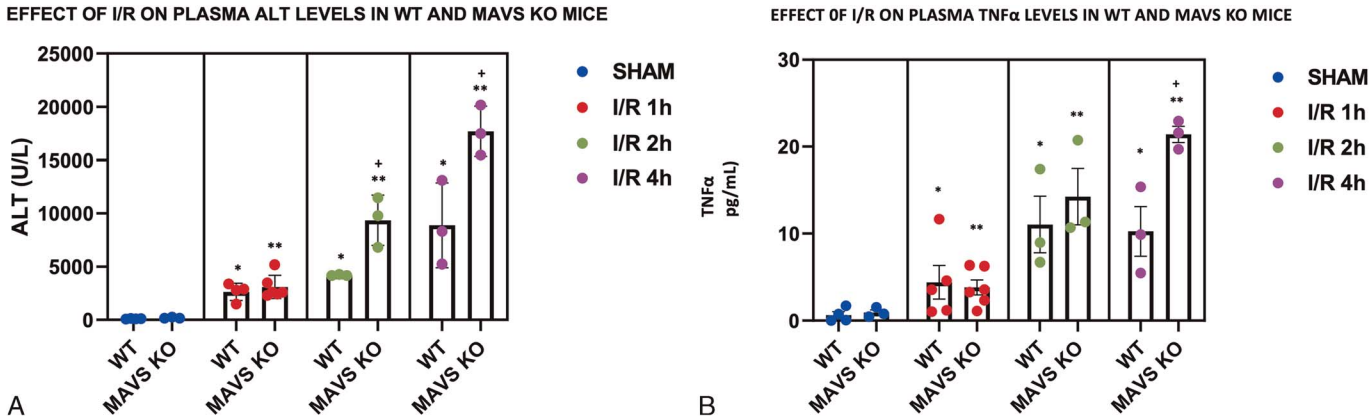

FIG. 4. **Effect of I/R on plasma ALT and TNF-α levels of WT and MAVS KO mice.** A, Note gradual increase in plasma ALT both in WT and MAVS KO mice. Moreover, at 2 and 4 hours after reperfusion, the plasma ALT of MAVS KO animals is significantly higher compared with the WT mice. ANOVA, n = 3–6, *post hoc P* < 0.05: *vs. WT sham, **vs. KO sham, $^{+}$vs. WT at 2 and 4 hours. B, TNF-α plasma levels at varying times after reperfusion. In WT mice, the TNF-α levels reach a plateau after 2 hours, whereas in MAVS KO mice, TNF-α continues to increase up to the 4 hours after reperfusion that was measured. At 4 hours, the levels of plasma TNF-α of MAVS KO mice are significantly higher than those of the WT mice. ANOVA, n = 3–6, *post hoc P* < 0.05: *vs. WT sham, **vs. KO sham, $^{+}$vs. WT at 4 hours.

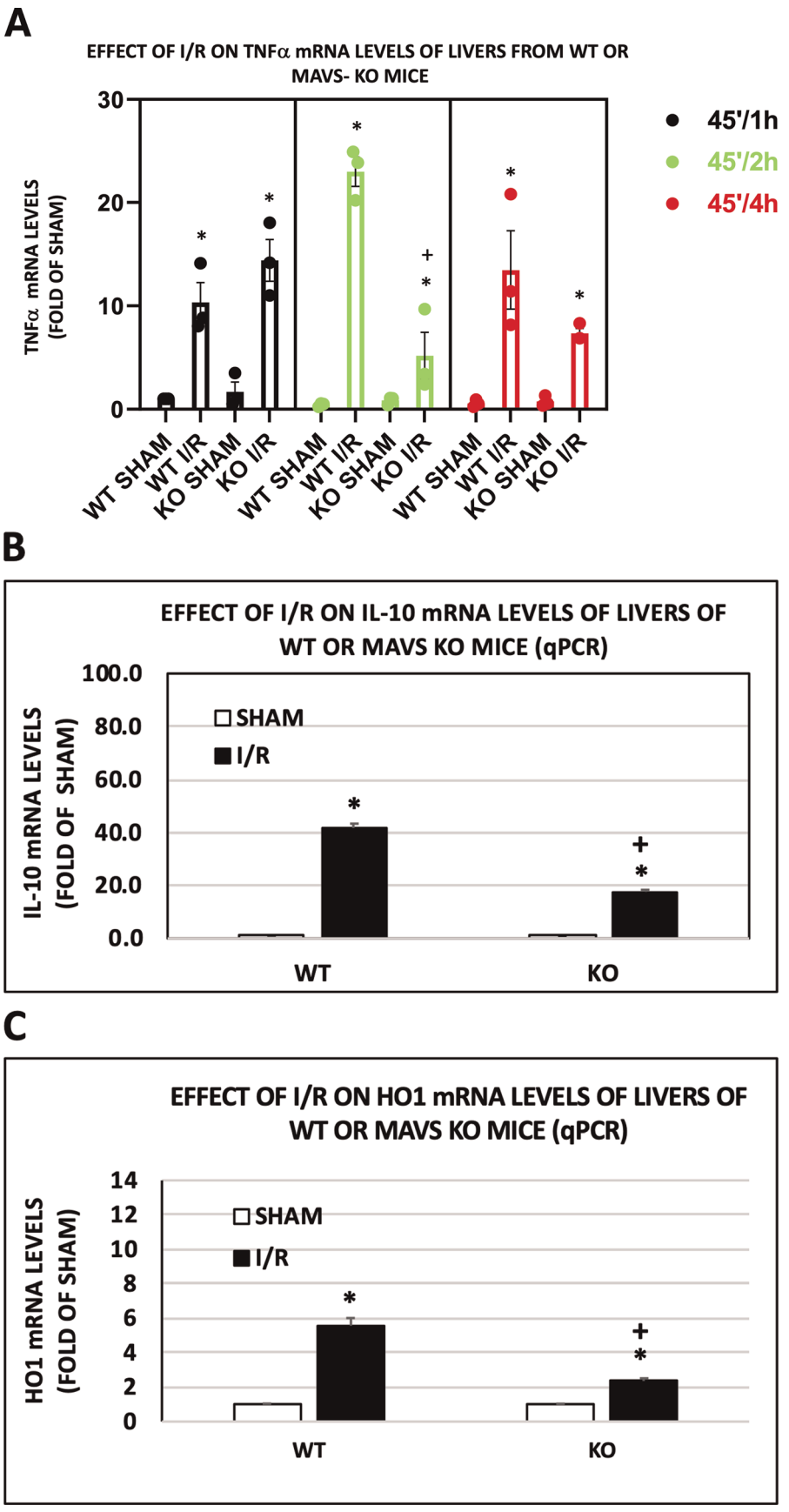

Fig. 5. **Effect of I/R on TNF-α, IL-10, and HO-1 mRNA levels in livers of WT or MAVS KO mice.** mRNA levels were assessed utilizing RT–quantitative PCR. **A**, TNF-α mRNA at varying times after reperfusion. *Post hoc* at $P < 0.05$: *vs. sham at corresponding hours, +vs. WT I/R at 2 hours, n = 3. Note that the elevation of both IL-10 (B) and HO-1 (C) mRNA following I/R in the WT livers is attenuated in the livers of I/R-treated MAVS KO mice. ANOVA, n = 4. IL-10 and HO-1 *post hoc* $P < 0.05$: *vs. corresponding sham, +vs. I/R.

measured hepatocellular enzyme release following 45-minute ischemia at various times of reperfusion (1–4 hours), in the WT and MAVS KO mice. Consistent with prior work, liver I/R caused hepatocellular injury in WT mice as indicated by increased plasma ALT levels, rising as the time after reperfusion increased from 1 to 4 hours. In MAVS KO mice, I/R injury was accentuated at 2 and 4 hours of reperfusion (Fig. 4A). As a measure of systemic inflammation emanating from liver I/R, we measured the plasma TNF-α levels. Concurrent with augmented hepatocellular injury in KO mice, plasma levels of TNF-α were further elevated in KO mice compared with WT, achieving significance at 4 hours of reperfusion (Fig. 4B).

We examined changes in TNF-α mRNA over the 4 hours of reperfusion in both WT and KO animals (Fig. 5A). At 1 hour of reperfusion, TNF-α mRNA increased to comparable levels in both WT and KO animals, whereas at 2 hours' reperfusion, TNF-α mRNA levels were significantly lower in MAVS KO animals than in WT animals. At 4 hours of reperfusion, TNF-α mRNA remained lower in MAVS KO animals than in WT animals. Interestingly, the finding that TNF-α mRNA was less in MAVS KO animals compared with WT animals is at odds with the observation that plasma TNF-α in MAVS KO animals exceeded that observed in WT animals at 4 hours of reperfusion (see Discussion for further elaboration). IL-10 and HO-1 are counterinflammatory molecules, known to lessen I/R-induced injury in the liver (16,17). We hypothesized that MAVS might modulate the expression of these molecules, as a mechanism underlying increased injury in its absence. Figure 5, B and C, demonstrates that both IL-10 and HO-1 mRNA levels increased in the liver following I/R, as previously reported. In MAVS KO animals, however, the I/R-induced rise in both molecules was significantly reduced compared with WT animals.

Reduction in MAVS expression increases apoptosis and mitophagy

Apoptosis is a recognized contributor to hepatocellular injury following liver I/R (18). One of the primary apoptotic executioner protease caspase-3 has been shown to mediate apoptosis following H/R (19). We therefore wished to evaluate whether the presence of MAVS might impact on the activation of caspase-3. We used Western immunoblotting to detect caspase-3 activation *in vitro* using H/R and under control conditions or when MAVS expression was reduced by specific siRNA. As shown in Figure 6, A and B, knockdown of MAVS levels with MAVS siRNA significantly potentiated the H/R- induced caspase-3 activation. As a positive control, activation of caspase-3 with the potent apoptosis inducer STSP is also shown (Fig. 6A).

To substantiate our finding based on bulk measurements with single-cell assays, we also measured caspase-3 activity in RAW cells using NucView 488 Caspase-3 reagent. Our pilot studies indicated that the most comprehensive and representative measurement both qualitatively and quantitatively was achieved with ImageXpress confocal imaging (IXM) and used this technology for our experiments. We evaluated caspase-3 levels *in vitro* following H/R with and without MAVS depletion using specific siRNA. As shown in the Figure, Supplemental Digital Content 6, A and B, http://links.lww.com/SHK/B456, H/R increased levels of active caspase-3 compared with normoxic controls. Reduction of MAVS levels with specific siRNA further increased caspase-3 levels under H/R conditions.

Mitophagy is a cellular process that serves to clear dysfunctional mitochondria, thereby reducing the elaboration of mitochondria-derived ROS (20). In some studies, blocking mitophagy has been shown to augment injury. We asked whether impaired mitophagy may have contributed to enhanced hepatocellular injury in MAVS KO animals.

To start answering this question, we utilized our *in vitro* model. As shown in Figure 7A (compare the upper and lower panels on the left), H/R induced an increase in red puncta, consistent with a rise in mitophagolysosomes, and an increase in mitophagy. Interestingly, in MAVS-silenced cells, H/R induced a further increase in mitophagolysosomes and hence in mitophagy. This is quantitated in Figure 7B. Consistent with the increase in mitophagy and reduction in mitochondrial numbers, the mitochondrial protein TOM20 was also decreased in MAVS-silenced cells

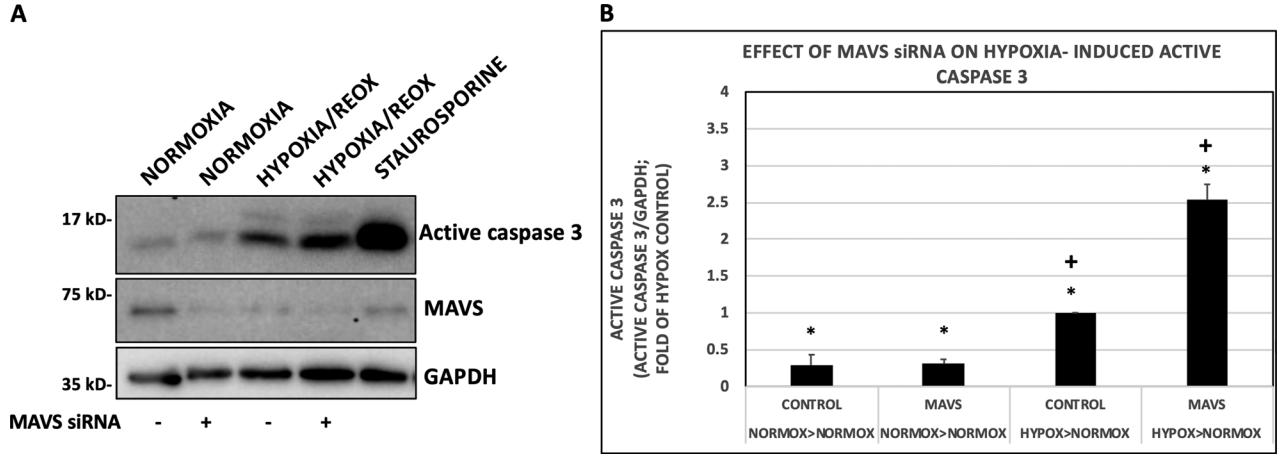

FIG. 6. **Reduction in MAVS expression enhances active caspase-3 levels in H/R- treated RAW cells using Western blots.** A, RAW cells were transfected with control or MAVS siRNA and after 24 hours were treated under hypoxia or normoxia conditions for 18 hours. Hypoxia cells were transferred to normoxia condition, and a set of normoxia cells was treated with STSP for 4 hours. Cell lysates were subjected to Western blots. Note that under hypoxia>reoxygenation conditions, active caspase-3 levels are enhanced compared with normoxia condition (lane 3), and reducing MAVS levels with specific siRNA further enhances caspase-3 levels in H/R-induced condition (lane 4) compared with control siRNA (lane 3). The utility of caspas-3 antibody is also demonstrated with the enhancement of caspase-3 following treatment with STSP (lane 5). B, Caspase-3 densitometry data were normalized to GAPDH levels for loading, and treatments were compared by normalizing to hypoxia>reoxygenation control siRNA. ANOVA, n = 7, *post hoc* $P < 0.05$: *vs. normoxia (control and MAVS siRNA) and hypoxia (MAVS siRNA), $^{+}$vs. normoxia (control and MAVS siRNA) and hypoxia control siRNA.

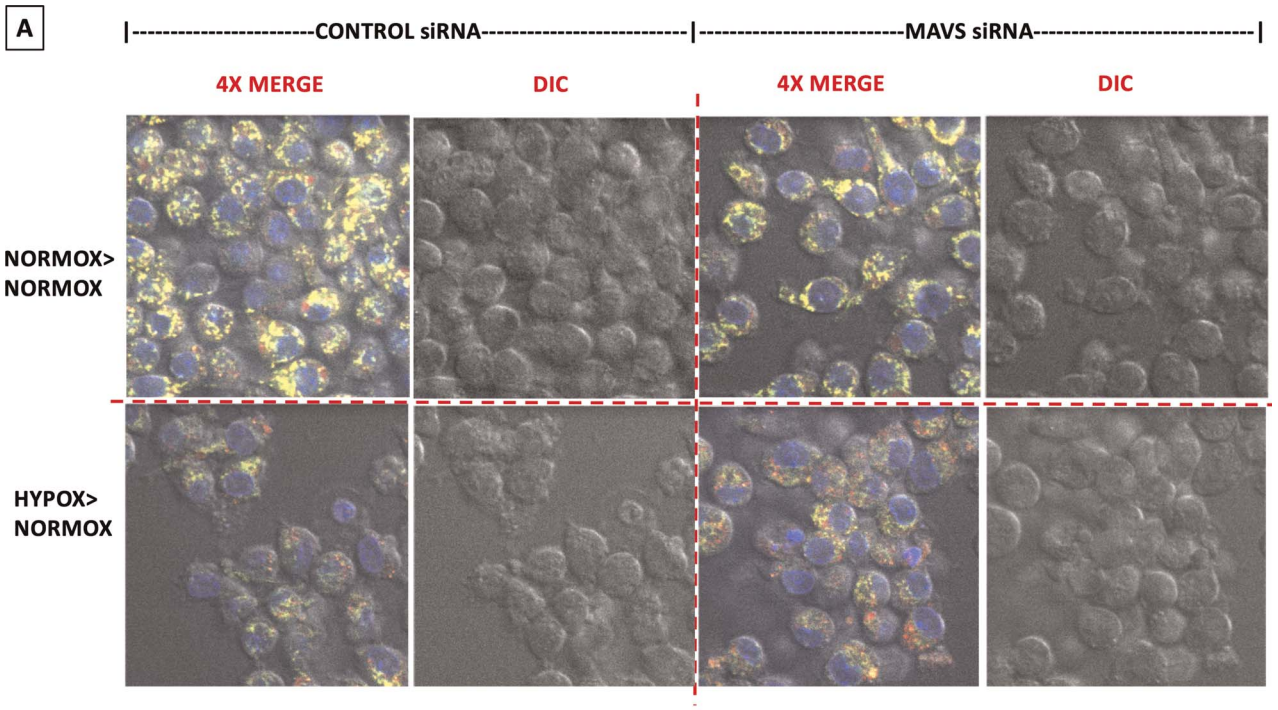

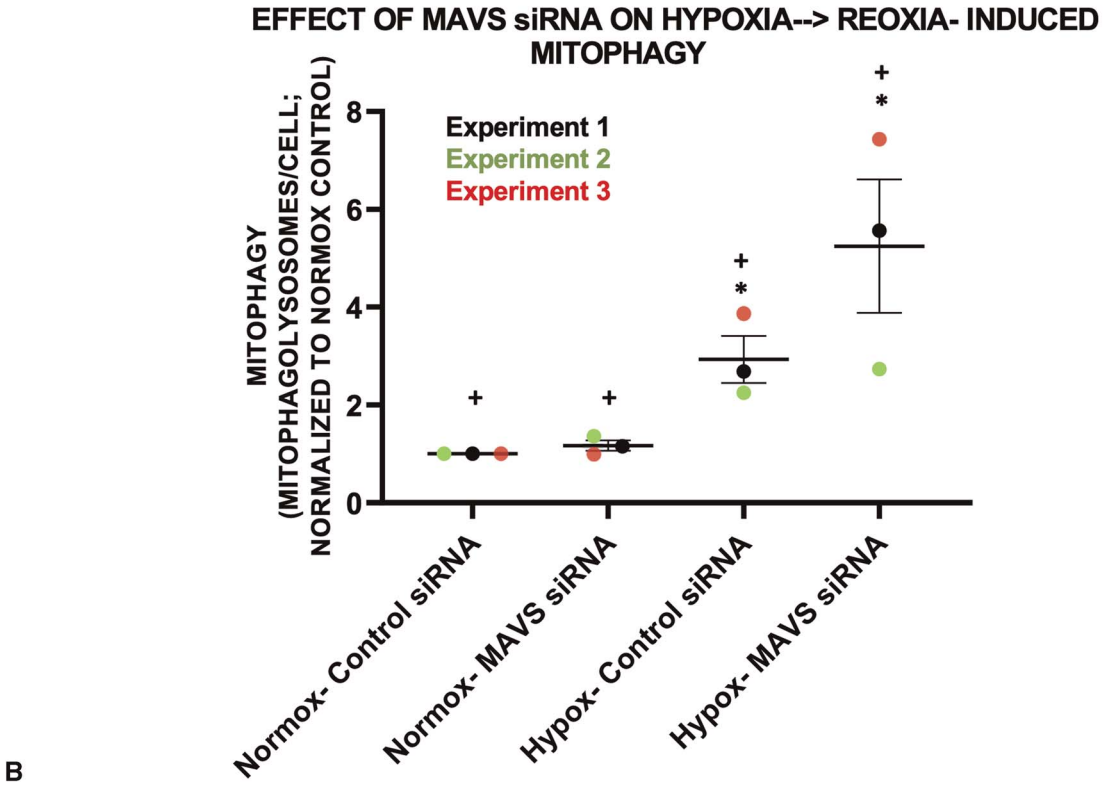

Fig. 7. **Reduction of MAVS levels increases H/R-induced mitophagolysosomes formation in RAW cells.** A, RAW 264.7 cell line, stably expressing plasmid mCherry-GFP-FIS1 (101–152) fusion protein, was transfected with specific MAVS or control siRNA. On the next day, cells were subjected to normoxia or hypoxia conditions for 18 hours followed by incubation for 4 hours under normoxia conditions. Cells were stained with nuclear stain Hoechst, mounted in TIRF microscope, and fluorescence photographed in the blue, green, and red channels, as well as light DIC; 4× merge composite of blue, green, red, and DIC. Note that control cells under hypoxia>reoxygenation (lower left) show red puncta, which are further enhanced when cells under hypoxia>reoxygenation were expressing lower levels of MAVS following treatment with MAVS- specific siRNA. The red puncta represent mitophagolysosomes. B, Red puncta on cell expressing more than three puncta were counted in three representative fields for each treatment divided by the total cell number and expressed as mitophagolysosome per cell. Shown are results for three separate experiments. ANOVA, n = 3. *Post hoc P* < 0.05: *vs. hypoxia MAVS siRNA, $^{+}$Normoxia vs. hypoxia.

subjected to H/R (Fig. 8A and quantitated in Fig. 8B). The mitophagy receptor protein, NIX/BNIP3L, was elevated in H/R treated MAVS-silenced cells (Fig. 8A and quantitated in Fig. 8C). Silencing of MAVS in cells in the absence of H/R had no effect on levels of TOM20 or NIX/BNIP3L (Figure, Supplemental Digital Content 7, http://links.lww.com/SHK/B457).

DISCUSSION

The outer mitochondrial protein MAVS is well known to be activated by viral infection and plays a central role in the generation of the mammalian antiviral response. However, a number of studies have suggested a role for MAVS activation in mediating the cellular response to nonviral stimuli (21,22). The present studies are the first to demonstrate that MAVS is activated by liver I/R through the generation of ROS and *via* a mechanism involving activation of the small GTPase protein Rac1. Interestingly, MAVS seems to exert a protective effect on the liver, reducing the magnitude of I/R-induced injury. Specifically, following liver I/R in MAVS-deficient animals, there was an increase in hepatocellular apoptosis, accompanied by a rise in plasma alanine aminotransaminase levels and TNF-α levels, when compared with wild-type animals. In the absence of MAVS, these effects were accompanied by a diminution of anti-inflammatory cytokines in the liver. We used a number of approaches to demonstrate that MAVS is activated by I/R whether applied *in vivo* or modeled *in vitro* with H/R. MAVS aggregation by SDD-AGE and reduction in the MAVS monomer both represent evidence of MAVS activation and were shown to occur following liver I/R. Hypoxia/reoxygenation caused reduction in MAVS monomer and also induced changes in the distribution of MAVS on the surface of mitochondria—the change in MAVS distribution mimicked that which we previously showed using the MAVS-activating agent dynasore. In addition, the morphology was comparable to that observed using poly I:C delivered by transfection, a known stimulus for MAVS, but not by naked poly I:C, which does not activate MAVS. In aggregate, these findings provide evidence that an I/R stimulus is able to activate MAVS.

Reactive oxygen species are generated during the process of I/R (8). In the current studies, we show that ROS contribute to MAVS activation *in vivo*. We previously showed that oxidative stress was able to induce MAVS *in vitro* (6). We extend these findings by showing that Rac1 activation seems to be a critical upstream event, as it is activated by H/R, and its pharmacological inhibition prevented MAVS activation. Rac1 has been shown to contribute to ROS generation both through the NADPH oxidase system and through mitochondrial ROS generation *via* an effect on the electron transfer to cytochrome c (14,15). Using specific inhibitors of both NADPH oxidase and also mitochondrial ROS, MAVS activation was reduced, suggesting that either or both were involved. The effect of apocynin seemed to be more robust, possibly due to superior *in vivo* kinetics or alternatively due to an antioxidant effect that was broader than on the NADPH oxidase alone. Work by Tal and colleagues (5) showed that ROS were able to activate RIG-I receptors, known to be involved in MAVS activation. In our prior work, dynasore, through generation of H_2O_2, activated MAVS in an RIG-I–independent manner. In the present studies, we did not evaluate the specific pathway whereby ROS activated MAVS, although this will be an important future study, given potential effects on downstream signaling.

We found it surprising that MAVS KO animals exhibited augmented hepatocellular injury and elevated plasma TNF-α levels following I/R compared with WT animals. We had anticipated that MAVS deletion would lessen the downstream inflammatory response, as has been observed after viral infection (23), as well as other contexts, such as folate-induced renal injury. The context-specific role of MAVS has been observed by other authors. For example, using bone marrow–derived macrophages, Li et al. (24) observed a differential cytokine response following MAVS deletion, depending on the stimulus. The elevation of TNF-α and interferon-β in response to extracts of feces RNA was significantly reduced in $MAVS^{-/-}$ cells, whereas induction of these cytokines by LPS was unaffected and thus seemed to be MAVS-independent. Finally, MAVS seems to play a role in maintaining epithelial barrier in the gastrointestinal tract following irradiation or immune-mediated tissue injury (25). Loss of epithelial barrier and transudation of intestinal factors into the portal system may have contributed to liver I/R injury in MAVS KO animals. Considered in aggregate, these findings suggest that the context in which MAVS becomes activated may be an important determinant of the downstream signaling events and its overall impact on injury. Mechanistically, it is conceivable that MAVS itself may be differentially modified, for example, by phosphorylation

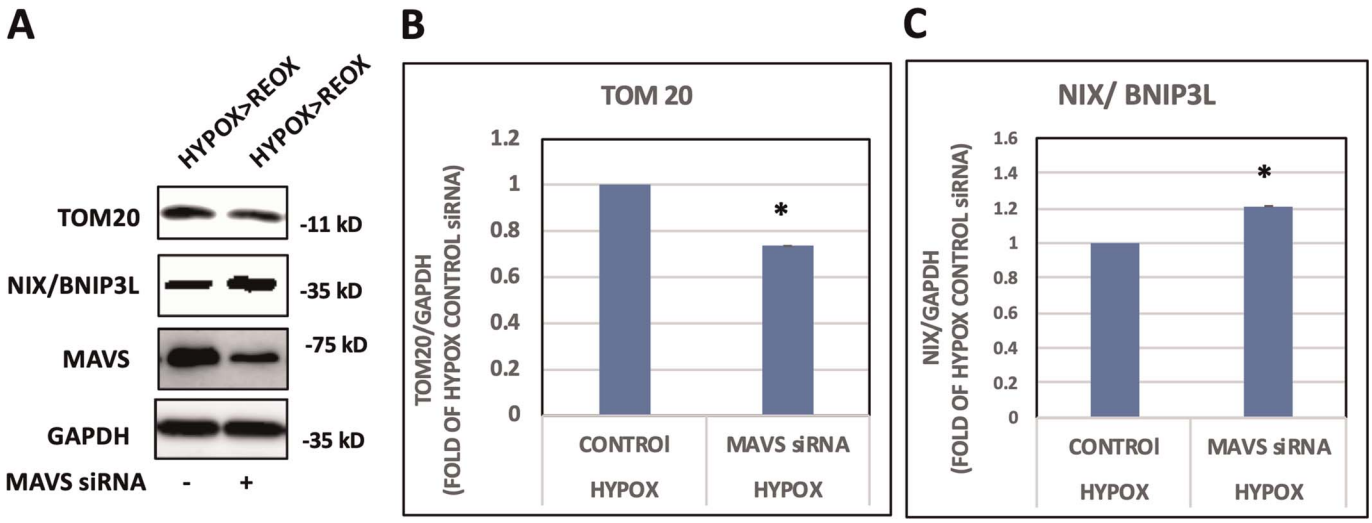

FIG. 8. **Effect of MAVS knockdown on H/R-induced mitophagy in RAW cells using Western immunoblots of TOM20 and NIX/ BNIP3L. RAW cells were transfected with control or MAVS siRNA and subjected to H/R or normoxia conditions.** A, Western immunoblot of TOM20, NIX/BNIP3L, MAVS, and GAPDH. B, Reduction in TOM20 levels in cells under H/R conditions after treatment with MAVS siRNA. **t* Test $P < 0.05$, n = 6. C, Increase in NIX/BNIP3L levels in cells under H/R conditions after treatment with MAVS siRNA. **t* Test $P < 0.05$, n = 7. Note reduction in MAVS levels following treatment with MAVS siRNA.

(26), or may interact with other proteins that modify its function, depending on the specific stimulus, and this may influence downstream events.

The plasma TNF-α levels in WT animals increased progressively during reperfusion, peaking at 2 hours and then subsiding. This time course of changes in TNF-α is consistent with those previously reported in response to I/R (27) and was also reflective of that observed for liver TNF-α mRNA. By contrast, the kinetics of plasma TNF-α observed for MAVS KO animals was different from WT animals in that the elevation persisted to the 4 hours' time point. Interestingly, in MAVS KO animals, the plasma TNF-α levels continue to rise even after the TNF-α mRNA levels subside. This differential response may be attributed to a number of potential causes. It is possible that release of TNF-α from the liver may differ between WT and MAVS KO animals, possibly due to differences in translation of Kupffer cells TNF-α mRNA. IL-10 has been shown to inhibit TNF-α mRNA translation (28). One might speculate that the reduction in IL-10 mRNA observed in MAVS KO animals following I/R might release this suppression and contribute to increased plasma levels of TNF-α protein. Alternatively, it is possible that other sources of TNF-α might be contributory. Splenic macrophages (29) exhibit increased TNF-α mRNA following hemorrhage/resuscitation and may potentially contribute to plasma TNF-α levels. Finally, as noted previously, MAVS is known to contribute to epithelial cell integrity in the gastrointestinal tract. Experimental colitis can lead to a rise in plasma TNF-α levels. In the absence of MAVS, the I/R stimulus may potentially have induced GI release of TNF-α systemically. Further, investigation will help to elucidate the underlying mechanism of augmented plasma TNF-α in this model.

I/R injury is known to induce mitochondrial dysfunction, leading to elaboration of excessive mitochondrial ROS and consequent tissue injury. We therefore asked whether impaired mitophagy in MAVS-deficient animals might have contributed to increased hepatocellular injury as failed clearance of dysfunctional mitochondria. Recent studies have shown that MAVS might directly serve as a mitophagy receptor, *via* its LC-3 binding motif "YxxI" (4). Conceivably, impaired mitophagy in the absence of MAVS might lead to an accumulation of dysfunctional mitochondria, with excessive generation and/or release of other mitochondrial factors, such as ROS, cytochrome c, and mitochondrial DNA, which could result in augmented cellular injury. Our data show that in the absence of MAVS, mitophagy in the *in vitro* H/R model was increased, as measured by reduction in total TOM20 levels and also by imaging of mitophagy in individual cells. The precise mechanism of this increase requires further study, although an increase in one mitophagic receptor NIX/BNIP3L was observed following H/R in MAVS-deficient RAW cells (Figure, Supplemental Digital Content 8, http://links.lww.com/SHK/B458). Although we had hypothesized that reduced mitophagy in the MAVS-silenced cells may have contributed to the increased hepatocellular injury, our studies showed that mitophagy was actually increased. It is possible, however, that this increase was not sufficient to address the increased injury in this group, and hence, increased cellular injury prevailed, despite measuring an overall increase in mitophagy.

In summary, the mitochondrial protein MAVS seems to have effects on inflammatory signaling beyond its classically described canonical antiviral activities. The current work presents a novel role for this molecule in the context of I/R injury. Future studies aimed at elucidating how MAVS activation in this setting is similar to and/or differs from its well-elucidated antiviral effects may prove useful in defining strategies to lessen injury.

ACKNOWLEDGMENTS

The authors thank Mr. Brent Steer for help with the hypoxic chamber experiments. The help of Ms. Donna Lyons of the vivarium at SMH with mice breeding and maintenance is greatly appreciated. The authors acknowledge the Keenan Research Centre Core Facilities at SMH for ongoing technical advice and expertise.

REFERENCES

1. Chan YK, Gack MU: Viral evasion of intracellular DNA and RNA sensing. *Nat Rev Immunol* 14:360–373, 2016.
2. El Maadidi S, Faletti L, Berg B, Wenzl C, Wieland K, Chen ZJ, Maurer U, Borner C: A novel mitochondrial MAVS/Caspase-8 platform links RNA virus-induced innate antiviral signaling to Bax/Bak-independent apoptosis. *J Immunol* 192: 1171–1183, 2017.
3. Subramanian N, Natarajan K, Clatworthy MR, Wang Z, Germain RN: The adapter MAVS promotes $NLRP_3$ mitochondrial localization and inflammasome activation. *Cell* 153:348–361, 2013.
4. Sun X, Sun L, Zhao Y, Li Y, Lin W, Chen D, Sun Q: MAVS maintains mitochondrial homeostasis *via* autophagy. *Cell Discov* 2:16024, 2016. doi:10.1038/celldisc.2016.24.
5. Tal MC, Sasai M, Lee HK, Yordy B, Shadel GS, Iwasaki A: Absence of autophagy results in reactive oxygen species–dependent amplification of RLR signaling. *PNAS* 106:2770–2775, 2009.
6. Ailenberg M, Di Ciano-Oliveira C, Szaszi K, Dan Q, Rozycki M, Kapus A, Rotstein OD: Dynasore enhances the formation of mitochondrial antiviral signalling aggregates and endocytosis-independent NF-κB activation. *Br J Pharmacol* 172: 3748–3763, 2015.
7. Buskiewicz A, Montgomery T, Yasewicz EC, Huber SA, Murphy MP, Hartley RC, Kelly R, Crow MK, Perl A, Budd RC, et al.: Reactive oxygen species induce virus-independent MAVS oligomerization in systemic lupus erythematosus. *Sci Signal* 9:ra115, 2016.
8. Galaris D, Barbouti A, Korantzopoulos P: Oxidative stress in hepatic ischemia-reperfusion injury: the role of antioxidants and Iron chelating compounds. *Curr Pharm Des* 12: 2875–2890, 2006.
9. Allen GFG, Toth R, James J, Ganley IG: Loss of iron triggers PINK1/Parkin-independent mitophagy. *EMBO Rep* 14:1127–1135, 2013.
10. Wang F, Birch SE, He R, Tawadros P, Szaszi K, Kapus A, Rotstein OD: Remote ischemic preconditioning by hindlimb occlusion prevents liver ischemic/reperfusion injury: the role of high mobility group-box 1. *Ann Surg* 251:292–299, 2010.
11. Dwight Z, Palais R, Wittwer CT: uMELT: prediction of high-resolution melting curves and dynamic melting profiles of PCR products in a rich web application. *Bioinformatics* 27:1019–1020, 2011.
12. Hou F, Sun L, Zheng H, Skaug B, Jiang Q-X, Chen ZJ: MAVS forms functional prion-like aggregates to activate and propagate antiviral innate immune response. *Cell* 146:448–461, 2011.
13. Xu H, He X, Zheng H, Huang LJ, Hou F, de la Cruz MJ, Borkowski B, Zhang X, Chen ZJ, et al.: Structural basis for the prion-like MAVS filaments in antiviral innate immunity. *Elife* 3:e01489, 2014.
14. Hordijk PL: Regulation of NADPH oxidases: the role of Rac proteins. *Circ Res* 98: 453–462, 2006.
15. Osborn-Heaford HL, Ryan AJ, Murthy S, Racila A-M, He C, Sieren JC, Spitz DR, Carte AB: Mitochondrial rac1 GTPase import and electron transfer from cytochrome c are required for pulmonary fibrosis. *J Biol Chem* 287:3301–3312, 2012.
16. Dinant S, Vetelainen RL, Florquin S, van Vliet AK, van Gulik TM: IL-10 attenuates hepatic I/R injury and promotes hepatocyte proliferation. *J Surg Res* 141:176–182, 2007.
17. Ke B, Shen XD, Gao F, Ji H, Qiao B, Zhai Y, Farmer DG, Busuttil RW, Kupoec-Weglinski JW: Adoptive transfer of ex vivo HO-1 modified bone marrow–derived macrophages prevents liver ischemia and reperfusion injury. *Mol Ther* 18:1019–1025, 2010.
18. Gujral JS, Bucci TJ, Farhood A, Jaeschke H: Mechanism of cell death during warm hepatic ischemia-reperfusion in rats: apoptosis or necrosis? *Hepatology* 33: 397–405, 2001.
19. Ho FY, Tsang WP, Kong SK, Kwok TT: The critical role of caspases activation in hypoxia/reoxygenation induced apoptosis. *Biochem Biophys Res Commun* 345: 1131–1137, 2006.
20. Pickles S, Vigié P, Youle RJ: Mitophagy and quality control mechanisms in mitochondrial maintenance. *Curr Biol* 28:R170–R185, 2018.

21. Yu CY, Chiang RL, Chang TH, Liao CL, Lin YL: The interferon stimulator mitochondrial antiviral signaling protein facilitates cell death by disrupting the mitochondrial membrane potential and by activating caspases. *J Virol* 84:2421–2431, 2010.
22. Guan K, Zheng T, Song T, He X, Xu C, Zhang Y, Ma S, Wang Y, Xu Q, Cang Y, et al: MAVS regulates apoptotic cell death by decreasing K48-linked ubiquitination of voltage-dependent anion channel 1. *Mol Cell Biol* 33:3137–3149, 2013.
23. Deng J, Chen Y, Liu G, Ren J, Go C, Ivanciuc T, Deepthi K, Casola A, Garofalo RP, Bao X: Mitochondrial antiviral-signalling protein plays an essential role in host immunity against human metapneumovirus. *J Gen Virol* 96:2104–2113, 2015.
24. Li X-D, Chiu Y-H, Ismail AS, Behrendt CL, Wight-Carter M, Hooper LV, Chen ZJ: Mitochondrial antiviral signaling protein (MAVS) monitors commensal bacteria and induces an immune response that prevents experimental colitis. *Proc Natl Acad Sci U S A* 18:17390–17395, 2011.
25. Fischer JC, Bscheider M, Eisenkolb G, Lin C-C, Wintges A, Otten V, Lindemans CA, Heidegger S, Rudelius M, Monette S, et al.: RIG-I/MAVS and STING signaling promote gut integrity during irradiation- and immune-mediated tissue injury. *Sci Transl Med* 9:eaag2513, 2017.
26. Liu S, Cai X, Wu J, Cong Q, Chen X, Li T, Du F, Ren J, Wu Y-T, Grishin NV, et al.: Phosphorylation of innate immune adaptor proteins MAVS, STING, and TRIF induces IRF3 activation. *Science* 347:aaa2630, 2015.
27. Colletti LM, Remick DG, Burtch GD, Kunkel SL, Strieter RM, Campbell DA Jr.: Role of tumor necrosis factor-alpha in the pathophysiologic alterations after hepatic ischemia/reperfusion injury in the rat. *J Clin Invest* 85:1936–1943, 1990.
28. Kontoyiannis D, Kotlyarov A, Carballo E, Alexopoulou L, Blackshear PJ, Gaestel M, Davis R, Flavell R, Kollias G: Interleukin-10 targets p38 MAPK to modulate ARE-dependent TNF mRNA translation and limit intestinal pathology. *EMBO J* 20:3760–3770, 2001.
29. Zhu XL, Zellweger R, Zhu XH, Ayala A, Chaudry IH: Cytokine gene expression in splenic macrophages and Kupffer cells following haemorrhage. *Cytokine* 7:8–14, 1995.